AD-A141 538 RESEARCH IN DENSE PLASMA ATOMIC PHYSICS(U) NAVAL 1/1
RESEARCH LAB WASHINGTON DC J DAVIS ET AL. 19 APR 84
NRL-MR-5311 SBI-AD-E000 570

UNCLASSIFIED F/G 20/9 NL

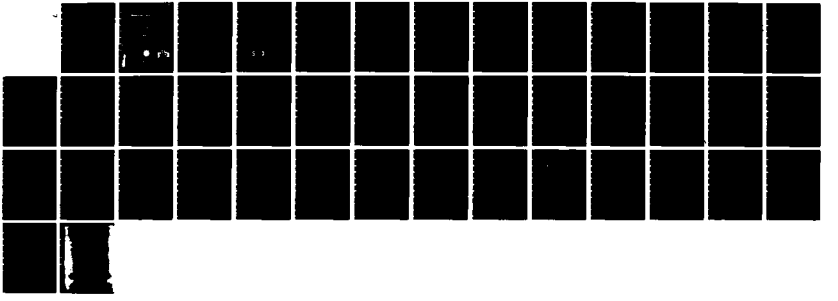

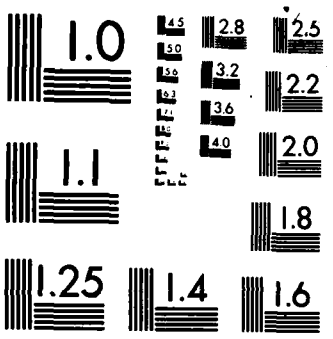

NRL Memorandum Report 5311

[illegible] Plasma Atomic Physics

J. DAVIS

Plasma Radiation Branch
Plasma Physics Division

M. BLAHA

[illegible], Dept. of Physics
[illegible], College Park, MD 20742

[illegible]

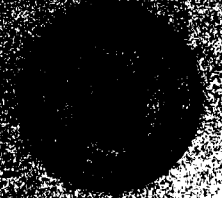

NAVAL RESEARCH LABORATORY
[illegible], D.C.

AD A111 538

SECURITY CLASSIFICATION OF THIS PAGE

REPORT DOCUMENTATION PAGE

1a REPORT SECURITY CLASSIFICATION UNCLASSIFIED	1b RESTRICTIVE MARK NOS
2a SECURITY CLASSIFICATION AUTHORITY	3 DISTRIBUTION/AVAILABILITY OF REPORT
2b DECLASSIFICATION/DOWNGRADING SCHEDULE	Approved for public release; distribution unlimited.
4 PERFORMING ORGANIZATION REPORT NUMBER(S) NRL Memorandum Report 5311	5. MONITORING ORGANIZATION REPORT NUMBER(S)
6a NAME OF PERFORMING ORGANIZATION Naval Research Laboratory 6b. OFFICE SYMBOL (If applicable) Code 4720	7a. NAME OF MONITORING ORGANIZATION
6c ADDRESS (City, State and ZIP Code) Washington, DC 20375	7b ADDRESS (City, State and ZIP Code)
8a NAME OF FUNDING/SPONSORING ORGANIZATION Office of Naval Research 8b OFFICE SYMBOL (If applicable)	9. PROCUREMENT INSTRUMENT IDENTIFICATION NUMBER
8c ADDRESS (City, State and ZIP Code) Arlington, VA 22217	10 SOURCE OF FUNDING NOS. PROGRAM ELEMENT NO: 61153N; PROJECT NO: RR011-09-41; TASK NO: ; WORK UNIT NO: 47-0911-04
11 TITLE (Include Security Classification) RESEARCH IN DENSE PLASMA ATOMIC PHYSICS	
12 PERSONAL AUTHOR(S) J. Davis, M. Blaha,* R. Cauble,** and U. Gupta**	
13a TYPE OF REPORT Interim 13b. TIME COVERED FROM 9/83 TO 10/83	14 DATE OF REPORT (Yr., Mo., Day) April 19, 1984 15 PAGE COUNT 40
16. SUPPLEMENTARY NOTATION *University of Maryland, College Park, MD 20742 **Berkeley Scholars, Inc., Springfield, VA 22151 This work was supported by the Office of Naval Research.	
17 COSATI CODES FIELD / GROUP / SUB GR	18. SUBJECT TERMS (Continue on reverse if necessary and identify by block number) Plasma, Dense, Atomic, Potentials

19 ABSTRACT (Continue on reverse if necessary and identify by block number)

The Density Functional Method (DFM) is examined for its applicability in describing density distributions and ionic configurations in dense plasma. These plasmas, where perturbation theories are not valid, can accurately be described by the hypernetted chain (HNC) potential. Comparison of results between the DFM and HNC model indicate that the DFM is valid even in strongly coupled plasmas. Other simpler models are found not to be valid in this regime. The Density Functional Method is applied to hydrogen-like argon ions in a hot, dense argon plasma to find energy level shifts and broadening by the plasma and electron collisions.

20 DISTRIBUTION/AVAILABILITY OF ABSTRACT UNCLASSIFIED UNLIMITED X SAME AS RPT ☐ DTIC USERS ☐	21 ABSTRACT SECURITY CLASSIFICATION UNCLASSIFIED
22a NAME OF RESPONSIBLE INDIVIDUAL J. Davis	22b TELEPHONE NUMBER (Include Area Code) (202) 767-3278 22c OFFICE SYMBOL Code 4720

DD FORM 1473, 83 APR EDITION OF 1 JAN 73 IS OBSOLETE

SECURITY CLASSIFICATION OF THIS PAGE

CONTENTS

I. INTRODUCTION 1

II. COMPARISON OF ATOMIC POTENTIALS FOR STRONGLY COUPLED NEON 2

III. LINE BROADENING AND IONIZATION IN DENSE ARGON PLASMAS ... 15

ACKNOWLEDGMENT 28

REFERENCES 38

RESEARCH IN DENSE PLASMA ATOMIC PHYISCS

I. Introduction

In recent years there has been considerable interest in studying plasmas at or above solid density because of its importance to radiation source development, inertial confinement fusion, and plasma spectrocopy. In addition to these areas of application, there is a more fundamental issue; that is, the modification of atomic properties and processes caused by the dense plasma medium. It is the purpose of this investigation to carry on in the spirit of our earlier investigations and focus attention on the solution to the time-independent Schrodinger equation with a self-consistent charge density.

For calculations of atomic properties the usual approach is to iteratively solve a set of coupled equations statistically describing the charge distributions and an effective electron-ion interaction potential. Incorporating this potential, the bound and free electron distributions are found from the Schrodinger equation. Thus, given an ion where the bound orbits are not externally specified, the solution of the equations directly gives orbital energy eigenvalues and (fractional) populations. The wave functions and the effective electrostatic potential obtained in this manner can be used to find spontaneous decay rates and cross sections for various atomic processes characterizing radiation, the spectrum of which can be employed to diagnose the plasma environment.

Herein we describe a method of calculating atomic properties of ions in a hot, dense plasma environment. Before we examine some results of this model, the Density Functional Method (DFM), we first examine the accuracy with which the DFM predicts density distributions and ionic configurations when the plasma is strongly coupled, i.e., when standard theoretical techniques can no longer be applied to arrive at a valid description of the plasma. The hypernetted chain (HNC) approximation for developing plasma density correlations, however, has been shown to be accurate in this regime. Thus a comparison of the DFM and HNC models for these dense plasmas is appropriate.

In Section II we describe the HNC method and a mechanism of developing an interionic potential from those results. Comparisons are made with the DFM as well as Debye and nearest neighbor approximations, for strongly

Manuscript approved February 9, 1984.

coupled neon. We end the section by concluding that the DFM remains a valid method even in strongly coupled plasma. Section III describes the Density Functional technique in some detail. Results of line shifts and broadening for hydrogenlike argon ions in strongly coupled argon plasmas are presented. These results include the effects of electron collisions.

II. Comparison Of Atomic Potentials For Strongly Coupled Neon

Thomas-Fermi and Hartree-Fock statistical models have been applied to highly ionized atoms in dense plasmas[1,2] and subsequently applied to a strongly coupled neon plasma.[3] However, ion correlations were neglected in these approaches. A self-consistent set of Schrodinger- Poisson equations including ion correlations was developed by Skupsky[4] to study the plasma microfield effects on a high-Z impurity ion embedded by a dense fully ionized low-Z plasma. An improvement over this method - the quantum mechanical treatment of the free electrons - was made by Davis and Blaha.[5] In a similar manner density functional theory (DFT) has been employed to investigate level shifts and screening effects in the impurity problem.[6,7]

The inclusion of ion correlations in these latter models is accomplished using a Boltzmann distribution under the assumption of nearly-classical ion interactions. In the case of the one-component plasma (dynamic ions in a neutralizing background charge), the assumption of a Boltzmann-like form for the ions would be erroneous for values of the ion coupling parameter,

$$\Gamma = \frac{(\bar{Z})^2 e^2 \beta}{r_o} ,$$

greater than about three.[8,9] Here $\bar{Z}$ is the effective ionic change, r_o is the ion sphere radius, and $\beta = 1/k_B T$. This discrepancy is not as significant for a "real" two-species plasma because the mobile electron fluid is able to provide more effective screening, but has yet to be investigated in the two-species model for $\Gamma > 2$ and for ions other than hydrogen. If one can utilize a model that is expected to provide accurate distributions for a strongly coupled system, one can also use that model to

examine the validity of using self-consistent statistical models in the strongly coupled regime.

Implicit in all the methods discussed here is the assumption that the lifetime of the ionic state is long enough so that the plasma has time to be polarized by the ion. Since the polarization (correlation) time is of the order of the inverse of the plasma frequency, all of the cases we are considering can be considered long-lived (a typical state lifetime -- the most rapid destruction mechanism being collisional de-excitation-- may be of the order of 10^{-14} - 10^{-15} s; ω_p^{-1} is about 10^{-17} s). Each model also assumes that since the ion state exists through many plasma periods, the concept of a time-averaged potential for atomic calculations is meaningful.

We investigate here the energy eigenvalues, charge distributions, and effective electron-ion potentials for strongly coupled neon plasmas using a self-consistent DFT model similar to that described in Ref. 7. These results are compared with those obtained from the solution of the two-component plasma hypernetted chain (HNC) equations, which are assumed to be valid at these densities and temperatures. The results will indicate the inadequacy of the Debye-Huckel (DH) and ion-sphere (IS) calculations when $13 \lesssim \Gamma \lesssim 1$.

Models

We consider an ion of nuclear charge Z in a plasma in which the average effective charge is $\bar{Z}$. $\bar{Z}$ is equal to Z minus the mean number of bound electrons per ion and is a result of the model. Density functional theory leads to a system of equations that must be solved self-consistently. The electrostatic potential is given by the Poisson equation,

$$V(r) = \frac{Ze^2}{r} + 4\pi e^2 \left[\frac{1}{r} \int_o^r dr\, r^2 (\rho_e+\rho_b+\rho_i) + \int_r^\infty dr\, r\, (\rho_e+\rho_b+\rho_i) \right]. \quad (1)$$

The plasma is assumed to be in thermal equilibrium and all electrical charge distributions are assumed to be spherically symmetric. In Eq. (1), ρ_b is the local density of bound electrons found from solving the Schrodinger equation where the interaction potential is V(r) from Eq. (1) with ρ_b set equal to zero.

ρ_e is the local charge density of free electrons. It is represented by a Fermi-Dirac energy distribution beyond a spherical boundary large enough so that the plasma at the boundary may be considered neutral. Inside this sphere the free electrons may be treated quantum-mechanically and are described by wave functions that are solutions of the time-independent Schrodinger equation. The ion charge density is assumed to take the Boltzmann form

$$\rho_i = \frac{n_e}{Z} \; e^{-\beta V(r)} \tag{2}$$

At $r = \infty$, $\rho_i = -\rho_e$, insuring neutrality; we also have appropriate boundary conditions. The equation are solved self-consistently with these boundary conditions to yield ρ_e, ρ_i, V(r), and the energy eigenvalues.

In order to gauge the reliability of the above model in a strongly coupled plasma we turn to a semiclassical treatment of particle correlations that has been found to accurately reproduce molecular-dynamics calculations in this regime. In this approach - the two-component plasma (TCP) - the ions and electrons are treated as classical particles that interact through effective two-body potentials which deviate from pure Coulomb behavior at short distances such that the essential quantum diffraction effects are simulated. A particular form has been suggested by Deutsch[10] and used in the computer simulations[11]. This form uses the reduced mass de Broglie wavelength, $\lambda_{\alpha\beta}$, where α and β are species labels, as a quantum mechanical cutoff parameter, i.e.

$$V_{\alpha\beta}(r) = \frac{\zeta_\alpha \zeta_\beta e^2}{r} \left[1 - \exp\left(-r/\lambda_{\alpha\beta}\right)\right]; \tag{3}$$

ζ_α is the charge of species α and $\lambda_{\alpha\beta} = h/(2\pi\mu_{\alpha\beta}k_\beta T)^{1/2}$ where $\mu_{\alpha\beta}$ is the reduced mass. This potential is finite at the origin and is expected to give reasonable results for nondegenerate plasmas so long as $\lambda_{ee}/r_o \ll 1$

(λ_{ee} is the smallest of the three $\lambda_{\alpha\beta}$.) This condition is equivalent to $\Gamma \ll 9\ (\bar{Z})^2/(T_{eV})^{1/2}$.

In order to include the plasma many-body effects, the binary interactions defined in Eq. (3) are used in the hypernetted chain (HNC) equations.[12] This is an approximate integral equation method for calculating static correlation functions for systems of particles with long range potentials and has proven to be accurate for strongly coupled hydrogen plasmas.[11] The quantities of interest are the radial distribution functions (rdf's), $g_{\alpha\beta}(r)$, which contain the static structural information in the TCP. The HNC approximation for the rdf's is

$$g_{\alpha\beta}(r) = \exp\ [-\beta V_{\alpha\beta}(r) + h_{\alpha\beta}(r) - c_{\alpha\beta}(r)], \tag{4}$$

where the total correlations

$$h_{\alpha\beta}(r) = g_{\alpha\beta}(r) - 1 \tag{5}$$

are related to the direct correlations $c_{\alpha\beta}$ by the Ornstein-Zernicke equations

$$\tilde{h}_{\alpha\beta}(k) = \tilde{c}_{\alpha\beta}(k) + \sum_{\gamma}^{i,e} \tilde{h}_{\alpha\gamma}(k)\ \tilde{c}_{\gamma\beta}(k). \tag{6}$$

Here the Fourier transform is defined as

$$\tilde{h}_{\alpha\beta}(k) = 4\pi n_{\alpha} \int_0^{\infty} dr\ r^2\ \frac{\sin kr}{kr}\ h_{\alpha\beta}(r). \tag{7}$$

Eqs. (4-7) are solved iteratively for $\alpha,\beta = i,e$. The rdf's generated by this procedure reduce to their Debye-Huckel (DH) forms in the limit of weak coupling ($\Gamma \ll 1$), but are considerably different from the DH approximation when Γ is order one or larger.

The TCP is a model system of point charges, ions with charge $+\bar{Z}$ and free electrons with charge -1. Formally the HNC scheme requires the exact $\bar{Z}$ as an input parameter; this is necessary if the ionic and electronic distribuiton functions are to be examined. In order to find the effective potential, however, only a rough guess of $\bar{Z}$ will suffice to determine much of the V(r) curve.

The effective electron-ion potential and the screening function, $\tilde{\epsilon}^{-1}(k)$, are defined via Poisson's equation, the Fourier transform of which is given by

$$V_{HNC}(k) = \frac{4\pi e^2 Z}{k^2 \tilde{\epsilon}(k)} = \frac{4\pi e^2 Z}{k^2} \left[\tilde{S}_{ii}(k) - \tilde{S}_{ie}(k)/\sqrt{\bar{Z}}\right] \tag{8}$$

The static structure factors are defined by

$$\tilde{S}_{\alpha\beta}(k) = \delta_{\alpha\beta} + (|\zeta_\alpha \zeta_\beta|)^{1/2} \tilde{h}_{\alpha\beta}(k) \ . \tag{9}$$

Close to a test point ion of charge $\bar{Z}$ the free electron distribution determines $V_{HNC}(r)$; the ion-ion rdf is negligible out to a distance of about one-half r_o. In this region Poisson's equation is

$$\nabla^2 V'_{HNC}(r) = 4\pi e^2 \bar{Z} \left[\delta(r) - \frac{n_e}{\bar{Z}} h_{ie}(r)\right], \quad r \lesssim r_o/2, \tag{10}$$

where the prime on $V_{HNC}(r)$ indicates the test ion has charge $\bar{Z}$, not Z. For a given temperature and electron density, a higher value of $\bar{Z}$ simply pulls the electron distribution, $h_{ie}(r)$, in tighter, an effect that essentially compensates the $\bar{Z}$ prefactor to h_{ie}. The result is that the function in brackets in Eq. (10) is very nearly insensitive to the mean ionic charge, i.e.

$$V'_{HNC}(r) = 4\pi e^2 \bar{Z} f(r) \tag{11}$$

where f(r) is a function nearly independent of $\bar{Z}$. This is the rationale behind the form of the potential in Eq. (8); $V_{HNC}(r)$ is a screening function dependent on density and temperature scaled by the nuclear charge Z. We find that this form very nearly reproduces the potentials found in the quantum-mechanical self-consistent model described earlier.

If the particle distributions are required (an accurate value of $\bar{Z}$ is needed to obtain the actual distributions) two steps are necessary. First, a guess of $\bar{Z}$ is made and the HNC equations solved for $\tilde{S}_{ii}(k)$ and $\tilde{S}_{ie}(k)$.

A "guess" of the potential is then found from Eq. (8). This potential can then be used in the Schrödinger equation to find wave functions for all bound states. The integrated wave functions provide a new $\bar{Z}$, in which, when used in the HNC code a second time, provide a new potential and the needed distributions. Generally only the one such iteration is required.

The definition[13] of V(r) in Eq. (8) implies a form of the dielectric function significantly different from that obtained using the fluctuation-dissipation theorm[14] (FDT), although both forms reduce to DH forms in the proper limits. For dense plasmas V_{HNC} from Eq. (8) agrees much more closely with results from the ion sphere model (described below) and with Thomas-Fermi[3] calculations, as well as the "potential of mean force" approximation, $V_{MF}(r) = \frac{Ze^2}{r} \ln [g_{ei}(r)]$, than an effective interaction derived from the FDT. In fact $V_{FDT}(r)$ shows screening that everywhere has a larger magnitude than $V_{DH}(r)$. The Debye potential itself is known already to predict excessive screening in plasmas where the validity of the DH approximation is questionable. A plasma in a near metallic state (where the ion sphere model might be used) shows a form very similar to the potential defined via Poisson's equation, which is qualitatively and quantitatively distinct from an effective interaction derived from the FDT.

As the plasma approaches the limit of a solid structure, the ion-sphere (IS) approximation becomes more valid. The ion-sphere model[4,15] assumes complete ion shielding within an ion-sphere radius by a uniform cloud of electrons. Poisson's equation in this case yields

$$V_{IS}(r) = Ze^2 \left[\frac{1}{r} - \frac{1}{2r_o} \left(3 - \frac{r^2}{r_o^2}\right) \right] . \qquad (12)$$

Results

We consider a strongly coupled neon gas plasma. Table I summarizes the conditions under which the runs were made, the value of $\bar{Z}$ being a result of the self-consistent density functional (DF) model. All cases have Γ's in excess of two. We note that both the HNC and DF models

Table I

Summary of selected neon plasma conditions described by the models. $\bar{Z}$ is the mean charge per ion. Γ is the ion coupling parameter.

Electron Density (cm^{-3})	Temperature (eV)	$\bar{Z}$	Γ
10^{24}	400	8.77	2.2
2.10^{24}	250	7.61	3.4
5.10^{24}	250	7.85	4.9
5.10^{25}	210	8.02	13.1

reduce to correct Debye-Hückel results in the limit of weak coupling ($\Gamma \ll 1$).

The ion charge density from the self-consistent model normalized to the backround density, $\rho_i/\rho(\infty)$, is equivalent to the ion-ion radial distribution function, g_{ii}. Fig. 1 displays the ion distributions resulting from DF solutions for the $\Gamma = 2.2$ and $\Gamma = 4.9$ cases. These figures are compared with g_{ii} from the HNC approximation using the effective binary interaction in Eq. (3) and with the Debye form

$$g_{ii}^{DH}(r) = \exp\left[-\frac{\bar{Z}e^2}{r} e^{-r/\lambda_D} \right] , \tag{13}$$

where

$$\lambda_D^{-2} = 4\pi n_e e^2 (\bar{Z}+1)\beta . \tag{14}$$

g_{ii}^{DH} shows the tendency of the DH approximation to excessively screen the ions in dense plasma, an effect previously seen in the OCP[8,16] and the TCP[11]. The HNC rdf is assumed to be the most accurate of the three representations, because, since $\lambda_{ii}/r_o \simeq 10^{-5}$, the ions are essentially classical particles and the computer simulations have supported the use of the HNC approximation for classical systems. In spite of the fact that ρ_i in the DF method - Eq. (3) - cannot reproduce the oscillations around $g_{ii} = 1.0$ for $2 \lesssim r/a_o \lesssim 4$ in the larger Γ case, the agreement between DFM and HNC even at $\Gamma = 4.9$ is very good. The small difference between these two forms is not expected to alter the effective potential[17]; we will test the significance of the difference below.

Fig. 2 compares the electron density profile (including both bound and free electrons) provided by the self-consistent method around an ion with the ion-electron radial distribution function produced by the HNC code for $\Gamma = 2.2$. The profiles are very close for $r/a_o \gtrsim 0.25$. The innermost r-point calculated on the Fourier transform mesh in the HNC code is $r/a_o = 0.125$. This also corresponds to the innermost r-mesh point of the potential, since $rV(r)/_{r=0} = Z$, interpolation between $r = 0$ and the first mesh point is possible for $V_{HNC}(r)$. Extrapolation of the HNC g_{ie} to smaller radii, however, would not be meaningful, since $\lambda_{ie}/a_o = 0.12$; thus quantum mechanical details are important in this region. Forrest Rogers has investigated this subject for hydrogen and few-times ionized

argon.[13] Since our goal is a many-body effective potential with which to examine average atom calculations, we find that the present model is adequate.

The DF effective potential is a consequence of the solution of the model. This function in the form $rV(r)$ appears in Fig. 3 for $\Gamma = 2.2$ and $\Gamma = 4.9$. The HNC/Poisson potential - Eq. (9) - is also presented. The two forms are seen to be very similar in both cases indicating the apparent validity of the quantum mechanical model even at very high densities. The Debye potential reveals much stronger screening except for large distances where $rV(r)$ tends to zero for all models.[18] The ion-sphere approximation is included for comparison: It agrees rather well with DFM and HNC/Poisson at short distances, but predicts even larger than Debye screening farther as r becomes larger - a tendency very much distinct from DFM and HNC. The overall form of the IS function is very different from the exponential behavior of the DH, DFM, and HNC/Poisson functions, a result of its constraint of fixed ionic volume.

Having now seen that the self-consistent formalism can provide reasonable results (compared with the HNC data) for these strongly coupled plasmas, we now look at the energy levels of the neon ions. Table II is a compilation of negative energy eigenvalues arising from the solution of the Schrodinger equation within the method. All negative (bound) energies are noted. The less deeply bound or absent DH values (resulting from more severe screening) as well as eigenvalues found by using $V_{IS}(r)$ and $V_{HNC}(r)$ are presented for comparison.

As a test of the significance of the difference between the two forms of the ion distribution functions - the DFM [Eq. (2)] and HNC [Eq. (4)] a run of the DF model was repeated for $\Gamma = 3.4$ using g_{ii}^{HNC} as a fixed function instead of Eq. (2). Those figures are set in parentheses in Table II. The difference is indeed minor and of the order of the numerical accuracy of the coded formalism.

As an example of a neon plasma at extreme conditions, we examined the case in which $n_e = 5 \cdot 10^{25} cm^{-3}$ and $T = 210$ eV, giving a Γ of 13.1. In this regime one expects to see considerable difference between the profiles produced by the DF and HNC methods. In Fig. 4 the ion distributions of the HNC, DF, and DH theories are reproduced. The HNC rdf shows that in this

TABLE II

Energy eigenvalues in atomic units of neon plasmas at Γ = 2.2, 3.4, 4.9, and 13.1 from self-consistent model (using g_{ii}^{HNC} in place of ρ_i^{SC} for the parenthetical values under Γ =3.4), and the HNC/Poisson model, Debye model, and ion-sphere model potentials. All bound level energies are given.

	Γ = 2.2				Γ = 3.4			
	DF	HNC	IS	DH	DF	HNC	IS	DH
1s	-42.3	-43.1	-43.8	-39.7	-34.6 (-34.6)	-39.4	-41.8	-33.7
2s	-6.15	-6.35	-6.45	-4.40	-2.88(-2.89)	-3.77	-4.65	-1.54
2p	-5.93	-6.24	-6.40	-4.00	-2.31(-2.41)	-3.41	-4.55	-0.77
3s	-0.64	-0.57	-0.23	-0.16				
3p	-0.50	-0.44	-0.12	-0.01				
3d	-0.22	-0.18						

	Γ = 4.9				Γ = 13.1			
	DF	HNC	IS	DH	DF	HNC	IS	DH
1s	-31.4	-34.1	-39.0	-25.8	-20.0	-21.5	-27.1	-0.66
2s	-1.30	-1.14	-2.40					
2p		-2.13						

case ion correlations are not Boltzmann-like. The non-negligible oscillation about $g_{ii} = 1$ shows that there is now a strong indication of ion ordering. Since the DF method utilizes Eq. (2), this effect is not seen in those results. Quantitatively the DFM and HNC rdf's are more dissimilar than the less coupled cases, although the DH curve is considerably more distinct from both of these.

Fig. 4 indicates that the effects of non-Boltzmann ion correlations are expected to be seen in the potential only at distances of r/a_o greater than one. Inside this radius the DFM and HNC ion distributions are similar enough that the potential, which here depends on the electron distribution, is not expected to be greatly affected. The Debye potential is expected to be overly screened again. Fig. 5 provides the calculated potentials for $\Gamma = 13.1$. The ordering seen in Fig. 4 is obviously manifested as the r-space oscillations in V(r). For purposes of atomic calculations, this effect will have little significance as the spatial extent of the 1s wave function is limited to the volume inside $r/a_o = 0.15$. For comparison we have plotted the ion sphere potential (crosses), which is seen to coincide closely with the DF and HNC effective potentials up to $r/a_o = 0.5$.

Our primary goal in this section is to investigate the applicability of the Density Functional Method to strongly coupled plasmas. As points of comparison we include potential calculations from Debye-Hückel (DH--correct for $\Gamma \ll 1$) and ion-sphere (IS--assumed correct for $\Gamma \gg 1$) approximations. The solution to the hypernetted chain (HNC) equations incorporating a semiclassical binary pseudopotential,[10] which has been found to be accurate in strongly coupled hydrogen plasmas,[11] is the plasma model whose statistical properties the DFM must mirror in order to be considered valid in this regime.

The DF method incorporates ion correlations via a Boltzmann factor with the self-consistent potential in the exponent. Although this form is approximate and cannot predict strong correlations which result in spatial oscillations in g_{ii}, the DF ion distribution is very close to the HNC profile for all cases considered with the exception of $\Gamma = 13$. The DH profiles predict more closely packed ions due to considerably more screening, a charateristic of DH theory outside of its range of validity and known to be incorrect.[8,11]

The IS profile (not depicted on Figs. 1 and 4) is a step function at r = r_o with amplitude zero inside this radius and amplitude one beyond r_o. This extreme form is not appropriate for the lower Γ cases, but is nearly correct for Γ = 13 (r_o=0.64a_o). Of course the structural oscillations are absent in the IS model but this should not be very important for calculations involving bound electrons.

The inner region of the effective potential is determined mainly by the electron distribution around the ion. The HNC and DFM electron distributions are seen in Fig. 2 to be close except very near the ion where the HNC solutions cannot be found. The ion sphere profile here possesses no structure, simply a horizontal line at g_{ie} = 1; this difference is crucial when developing the effective potential that is used to investigate the atomic structure of the ion.

The effective potential is a consequence of the solution of the DF method. The HNC interaction is derived from a screening function that is nearly independent of the average effective charge, $\bar{Z}$ (for a given temperature and density), scaled to the nuclear charge of the ions. The derivation of $V_{HNC}(r)$ is from Poisson's equation, not the fluctuation dissipation theorm as explained in the last section.

The DF potential is found to be very similar to $V_{HNC}(r)$ for the lower Γ cases. The HNC potential is less screened than the DF potential in the region $r \lesssim r_o/2$, where the electron distribution essentially determines the form of the potential. The electron "pile-up" near the nucleus is larger in the DF model, more effectively screening the positive charge. The DF electron distribution and thus the effective potential in this region are probably more accurate than the HNC results. For larger r, however, the ion distribution begins to effect the potential. The ion-ion rdf curves in Figs. 1 and 4 show the ions generally less packed in the HNC approximation than in the DF method, evidence of the greater "pile-up", but the structure is not simple. The enhanced (non-Boltzmann-like) ion correlations shorten the range of the calculated potential. The HNC potential in this region is probably the more accurate of the two.

Fig. 5 indicates the presence of very strong enhanced correlations effecting the potential. Using the HNC ion distributions in the DF method in place of the Boltzmann from does not allow $g_{ii}(r)$ to readjust to changes

in the electron distribution in each iteration (unless the HNC code is coupled directly to the DF scheme, a procedure we have not undertaken). Only in the $\Gamma = 13$ case might this be important. A potential constructed of the effective potential from the DF theory inside $r \approx r_o/2$ and $V_{HNC}(r)$ outside this point should suffice for most atomic calculations. For bound state energies at $\Gamma = 13$, the differences between HNC an DF are not important (see Table II). Calculations of continuum properties may be effected. This problem will be investigated in the future.

The inner region is more important for obtaining information on bound states. Here, the ion sphere approximation is hampered by the assumption of uniform electron density with the result the $V_{IS}(r)$ predicts more deeply bound states than HNC or DFM (which are in turn more deeply bound than the inappropriate DH values). This is true even at the extreme case of $\Gamma = 13.1$ as indicated by Table II. At the temperatures and densities for the cases listed, the HNC and DF potentials predict the same number of bound states with approximately the same energies. The IS approximation predicts more deeply bound inner levels but may result in less energetically bound outer levels (as in $\Gamma = 2.2$) if the wave functions extend into the region where the range of the IS potential is foreshortened by its definition of a fixed ionic volume. The Debye values all indicate more shallow states, because of large screening. (If in the definition of λ_D in Eq. (14), Z were used instead of $\bar{Z}$, the result would be even more severe screening. Setting $\bar{Z} = 0$ in Eq. (14) i.e., using the electron Debye length, produces a potential devoid of any ionic contributions to the correlation functions. The result here is a potential that lies much above all of the curves; this approximation provides too little screening.)

Since the HNC/Poisson potential appears to be accurate for atomic calculations in neon for $\Gamma \lesssim 2.2$ (by Fig. 3 and Table II), this approximation, which is very easy to generate, can be used to examine other properties of such strongly coupled systems requiring a many-body potential. For calculations at higher coupling and details of electron distributions very close to the nucleus, the self-consistent method is needed.

We have shown the self-consistent model produces reliable results for strongly coupled plasmas compared to hypernetted chain results in neon up to Γ of order five and higher if HNC ion distributions are employed. In addition, we have shown that the HNC method of generating correlation functions provides an effective potential that can be used in calculations of atomic properties up to Γ of order two (for neon). Debye-Huckel theory is not a meaningful approximation in strongly coupled plasmas. Nor can we recommend the use of the ion sphere potential for any of the cases examined here.

III. Line Broadening and Ionization in Dense Argon Plasmas

In this particular section considerations are made to obtain the binding energy of the electron in a given eigenstate via the Density Functional Method. In effect we consider the difference of total energies for the two specific configurations - one with the electron bound to the ion, and the other where it is ionized and contributes to the free electron plasma. As will be seen from the results, the binding energies calculated this way are significantly different from the usual procedure of generating eigenvalues in an effective potential.

The Density Functional Method (DFM)

In the present investigation we have studied energy levels, lowering of ionization potential, collision cross sections, and electron collision line broadening of hydrogen-like argon in pure argon plasma at T = 1000 eV and electron densities of 5×10^{24} and 2×10^{25} cm^{-3}.

Basic assumptions of our procedure are the spherical symmetry of electron and ion distribution around the central ion, continuous distribution of all charges around the given nucleus, and the time-independent character of wave functions describing both the bound and the free electrons.

The electron wave functions satisfy the equation (in atomic units which are used unless specified otherwise)

$$\left\{-\frac{1}{2}\nabla^2-\frac{Z}{r}-\int\frac{\rho(r')}{|\vec{r}-\vec{r}'|}\,d\vec{r}'+V_{xc}[n_e(r)]-V_{xc}[n_e(\infty)]\right\}\psi(\vec{r})=\varepsilon\psi(\vec{r}), \qquad (15)$$

where Z is the nuclear charge, ρ is the local charge density, n_e is the local electron density (including the bound and free electrons), and V_{xc} is the exchange-correlation contribution to the chemical potential of a uniform electron gas of density n_e. The wave function $\psi_{n\ell}$ of the bound electron in the $n\ell$ orbit is normalized to unity, while the continuum wave functions are normalized so that at large r,

$$\psi_k(\vec{r}) \to \exp\,[i\vec{k}\cdot\vec{r}] \qquad (16)$$

with $k^2 = 2\varepsilon$.

The local electron density n_e is calculated from the spherical average of $|\psi_{n\ell}|^2$ and $|\psi_k|^2$,

$$n_e(r) = |\psi_{n\ell}|^2_{av} + {}_0\int^{\infty} W(k)\,|\psi_k|^2_{av}\,dk, \qquad (17)$$

where $\pi^2 k^{-2} W(k)$ is the Fermi distribution function and

$$\int W(k)dk = n_e(\infty) \equiv N_e\ . \qquad (18)$$

Therefore $n_e(r) \to N_e$ at large distance from the central ion. The expression for V_{xc} was taken from Dharma-Wardana and Taylor[19] (see also Ref. 5). It is assumed that the ion distribution follows the Boltzmann statistics and that

$$n_i(r) = n_i(\infty)\exp[-V(r)\bar{Z}/k_BT]\ . \qquad (19)$$

k_B is the Boltzmann constant, T the temperature, $\bar{Z}$ is the effective charge of ions surrounding a given hydrogen-like ion, and

$$V(r) = \frac{Z}{r} + \int\frac{\rho(r')}{|\vec{r}-\vec{r}'|}\,d\vec{r}'\ . \qquad (20)$$

Finally, the local charge density ρ in (15) and (20) is given in terms of the electron and ion charge density ρ_e and ρ_i, respectively, by

$$\rho = \rho_e + \rho_i \ , \tag{21}$$

with

$$\rho_e = - n_e \ , \ \rho_i = \bar{Z} n_i \ .$$

In a neutral plasma, $n_e(\infty) = \bar{Z} n_i(\infty)$.

The present method differs from the procedure used in Ref. 5 in one important point. Here the electric charge density ρ in Eq. (15) is calculated from all charges and both the bound and free electrons move in the same potential. In Ref. 5 the self-interaction of the bound electron was not included in the equation for $\psi_{n\ell}$, and V_{xc} was calculated only from the density of free electrons. In the limit of very low densities N_e, our present method leads to incorrect asymptotic behavior of the potential terms in (15), because the exchange-correlation term does not fully compensate the self-energy contribution to (20). This difficulty is well known from the Hartree-Fock-Slater approximation for many-electron atoms[20], but it is of negligible importance for high-density plasmas.

The Eq. (15) has been solved self-consistently by an iterative procedure. Due to the high temperature and high nuclear charge Z, the expansion of ψ_k into partial waves requires inclusion of a large number of terms. To speed up the calculation and to reduce the number of contributing partial waves, we approximated the free electron density in the outer region by the expression

$$n_e = \sqrt{2}\, \pi^{-2} \int_{V'/kT}^{\infty} \sqrt{\varepsilon}\ \{ \exp[(\varepsilon - V' - \mu)/k_B T] + 1 \}^{-1}\, d\varepsilon \tag{22}$$

with

$$V'(r) = V(r) - V_{xc}[n_e(r)] + V_{xc}[n_e(\infty)] \ . \tag{23}$$

μ is the chemical potential determined by the condition that $n_e \to N_e$ for $r \to \infty$. The distance r_o, beyond which the electron density derived from the solution of (15) was replaced by (22), was chosen in such a way that at r_o the densities n_e obtained by both methods were in agreement. This condition does not uniquely determine r_o, however, because the electron density profile resulting from the solution of (15) exhibits oscillations with decreasing amplitude as r increases, while (22) is a smooth function

of r and it intersects the correct density profile in many points. In the outer region, (22) represents a good approximation to a smoothed profile of n_e and it was verified that atomic parameters derived from such density profile were in agreement with a full-scale calculation. The reliability of (22) in the outer region is demonstrated in Fig. 6 which shows a comparison of electron density profiles from the solution of Eq. (15) and from formula (22). In this particular case, $r_o = 0.555$ in the last iteration, and the electron density for $r > r_o$ (dashed curve) was obtained from (15) using a self-consistent potential of the last iteration.

The described procedure requires a knowledge of the effective charge $\bar{Z}$ appearing in the ion distribution (19). We have determined $\bar{Z}$ from the average atom model (AAM) using the density-functional theory for pure argon plasma at a given temperature and electron density. Many variations of the AAM have been described in the literature. They fall roughly into two categories depending on whether the AAM has or has not a definite boundary. In our method, the average atom is not spatially limited, and the computational scheme for the solution of the AAM is the same as for the hydrogen-like ion except for Eq. (17), where the term $|\psi_{n\ell}|^2_{av}$ should be replaced by

$$\sum_{n\ell} b_{n\ell} \; |\psi_{n\ell}|^2_{av} \; .$$

$b_{n\ell}$ are the occupation numbers of individual $n\ell$ levels obtained from the relation

$$b_{n\ell} = 2(2\ell+1)\{\exp[(\epsilon_{n\ell}-\mu)/k_B T]+1\}^{-1} \; . \qquad (24)$$

$\bar{Z}$ is then given by

$$\bar{Z} = Z - \sum_{n\ell} b_{n\ell} . \qquad (25)$$

Similarly to the case of a hydrogenic ion, Eqs. (15), (17), (19) and (21) should be solved self-consistently and Eqs. (24) and (25) have to be satisfied. Results for two plasma conditions investigated in the present paper are given in Table III.

Table III

Characteristics of pure argon plasma conditions studied in this paper.

Temperature (eV)	1000	1000
Electron density (cm^{-3})	5×10^{24}	2×10^{25}
Effective ion charge $\bar{Z}$	16.08	15.46
Coupling constant	4.07	6.04
Debye length $D(a_o)$	0.480	0.245
Ion sphere radius $R_i(a_o)$	1.730	1.076

The validity of Boltzmann statistics for ion distribution (19) in a plasma with the ion-coupling parameter $\Gamma > 1$ may be questionable, but a comparison with the hypernetted chain approximation (Fig. 7) indicates that even at this Γ the Boltzmann distribution is still an acceptable approximation.

Results and Discussion

For plasma conditions considered in this paper, the Debye length is much smaller than the ion sphere radius (Table III) and consequently one can expect that the Debye-Hückel theory would be inadequate for the description of plasma properties. This is demonstrated by comparison of potentials in Fig. 8. The DH potential is substantially lower than the self-consistent potentials for either the AAM or the hydrogen-like ions, and the one-electron eigenvalues $\varepsilon_{n\ell}$ are correspondingly higher. Table IV shows a comparison of eigenvalues $\varepsilon_{n\ell}$ for the bound electron in the AAM, in the linearized DH potential, in the hydrogen-like argon ion from the solution of Eq. (15), and for an isolated H-like ion. The occupation numbers $b_{n\ell}$ for levels in the AAM are also shown. The highest bound levels in the AAM and in the H-like ions are 3d and 2p for electron densities 5×10^{24} and 2×10^{25} cm^{-3}, respectively, but only 3s and 2s in the DH potential.

In considering the energy differences between various excited levels of the ion, one has to add to the energy of the bound electron the energy of the surrounding plasma which also depends on the level $n\ell$. Let R' be the distance from the nucleus of a given hydrogenic ion such that for $r>R'$, $n_e(r) = N_e$, $n_i(r) = N_e/\bar{Z}$, and $V(r) = 0$. Assuming that the ions obey Boltzmann statistics, the total energy $E_{n\ell}$ of an ion in the $n\ell$ state and the plasma inside a sphere with the radius R' is

$$E_{n\ell} = \varepsilon_{n\ell} + N_e\int_0^\infty \tfrac{1}{2}k^2 W(k)|\psi_k|^2_{av}\, dk d\vec{r} + \int \frac{Z}{r}\rho_i d\vec{r}$$

$$+ \frac{1}{2}\int(\rho_i-\rho_e)\int \frac{\rho(r')}{|\vec{r}-\vec{r}'|}\, d\vec{r}' d\vec{r} \qquad (26)$$

Table IV

Energy levels (at. units) in pure argon plasma at T = 1000 eV.

Level	Isolated hydrogen-like argon	$N_e = 5 \times 10^{24}$ cm^{-3}					$N_e = 2 \times 10^{25}$ cm^{-3}				
		Average atom model		Hydrogen-like argon			Average atom model		Hydrogen-like argon		
	$\varepsilon_{n\ell}$	$b_{n\ell}$	$\varepsilon_{n\ell}$ (from eq.(1))	$\varepsilon_{n\ell}$ (from DH potential)	$\varepsilon_{n\ell}$ (from eq.(1))	$I_{n\ell}$ (from eq.(13))	$b_{n\ell}$	$\varepsilon_{n\ell}$ (from eq.(1))	$\varepsilon_{n\ell}$ (from DH potential	$\varepsilon_{n\ell}$ (from eq.(1))	$I_{n\ell}$ (from eq.(13))
1s	-162.0	1.060	-138.1	-127.6	-140.1	-148.2	1.512	-123.3	-99.5	-130.6	-140.6
2s	- 40.5	0.092	- 22.3	- 13.6	- 24.6	- 28.4	0.264	- 12.6	- 2.16	- 16.2	- 21.3
2p	- 40.5	0.271	- 21.6	- 12.2	- 24.1	- 28.3	0.769	- 11.3	-	- 15.5	- 21.0
3s	- 18.0	0.056	- 3.39	- 0.358	- 4.41	- 6.6	-	-	-	-	-
3p	- 18.0	0.167	- 3.04	-	- 4.16	- 6.5	-	-	-	-	-
3d	- 18.0	0.273	- 2.44	-	- 3.59	- 6.3	-	-	-	-	-

$$+ \int n_e \{V_{xc}[n_e(\infty)] - V_{xc}[n_e(r)] + f_{xc}[n_e(r)]\}\, d\vec{r} + \frac{3}{2} k_B T \int n_i d\vec{r} + TS.$$

f_{xc} is the exchange and correlation energy per electron of a uniform electron gas of density n_e, and it is related to V_{xc} by

$$V_{xc} = d\,[n_e f_{xc}(n_e)]/dn_e.$$

S is the entropy of the system inside R′. In evaluating (26) for different nℓ, R′ should be such that the total number of particles inside R′ remains the same. Terms involving $\int n_e\, d\vec{r}$ and $\int n_i\, d\vec{r}$ then cancel out in energy differences. We also omit small contributions arising from differences of the terms $\int n_e(f_{xc} - V_{xc})\, d\vec{r} + TS$ in (26).

The total energy E_∞ of a fully ionized atom can be obtained by the same procedure, if the term $|\psi_{n\ell}|^2_{av}$ in Eq. (17) is omitted altogether. The charge density distribution in this case differs from the distribution for a hydrogenic ion. The negative ionization energy of the nℓ H-like level is then equal to

$$I_{n\ell} = E_{n\ell} - E_\infty + \frac{3}{2} k_B T, \qquad (27)$$

where the last term represents the energy necessary for the thermalization of the ejected electron. The values of $I_{n\ell}$ are shown in Table IV.

In Table V, we compare the lowering ΔI of ionization potential for individual nℓ levels derived from Eq. (27), from eigenvalues of the H-like ion in the Debye-Huckel potential, from the Stewart-Pyatt formula[21], from the temperature independent, uniform electron density ion sphere model ($\Delta I = -\frac{3}{2}(Z-1)/R_i$, R_i = ion sphere radius), and from the DH formula $\Delta I = -Z/D$. The value D of the Debye screening length was taken from Table III. R_i corresponds to the hydrogenic ion with a charge Z-1 = 17.0, and is therefore slightly larger than values in Table III. The agreement between our present results and the Stewart-Pyatt formula or the ion sphere model is very good which can be understood by comparing the density profiles in Figs. 6 and 7. Substantial deviations from a uniform electron density take place only in the inner region of the ion sphere, and the ion density profile is steep at the ion sphere boundary.

Table V

Lowering of ionization potential for H-like argon at 1000 eV.

Level	$N_e = 5 \times 10^{24}$ cm^{-3}		$N_e = 2 \times 10^{25}$ cm^{-3}	
	Present result (Eq.(13) and Table 1)	From $\varepsilon_{n\ell}$ in DH potential	Present result (Eq. (13) and Table 1)	From $\varepsilon_{n\ell}$ in DH potential
1s	-13.8	-34.4	-21.4	-62.5
2s	-12.1	-26.9	-19.2	-38.3
2p	-12.2	-28.3	-19.5	
3s	-11.4	-17.6		
3p	-11.5			
3d	-11.7			
Stewart-Pyatt	- 13.6		- 22.0	
Ion sphere model	- 14.5		- 23.0	
DH theory	- 37.5		- 73.5	

Lowering ΔI (at. units) of ionization potential for hydrogen-like argon. Pure argon plasma, T = 1000 eV.

The frequency shifts of the Lyman α and Lyman β lines obtained from values $I_{n\ell}$ in Table IV are -43.5 eV and -62.6 eV, respectively, for the electron density 5 x 10^{24} cm^{-3}, and the Lyman α shift for N_e = 2 x 10^{25} cm^{-3} is -51.7 eV. However, these shifts do not necessarily correspond to actual observable line shifts as mentioned in the conclusion. It is worth noting that shifts obtained in the present paper are much larger than shifts of an argon ion in a pure hydrogen plasma[4,5], but they are smaller than shifts derived from the eigenvalues $\varepsilon_{n\ell}$ only.

The optical transition probability coefficients A calculated from the standard formula using energy differences from Table IV and self-consistent bound wave functions are changed by plasma effects only slightly as indicated in Table VI.

The shift of spectral lines due to the plasma environment is accompanied by the line broadening. There are several mechanisms that participate in this process and we have restricted our investigation to the electron collison broadening effects. Assuming that the impact approximation is valid and that one can separate collision broadening effects from other mechanisms, the full width at half-maximum (FWHM) of a spectral line is given by

$$\text{FWHM} = q^{(\text{in})}_{(\text{upper})} + q^{(\text{in})}_{(\text{lower})} + N_e\{v \int |f_{\text{upper}}(\Omega) - f_{\text{lower}}(\Omega)|^2 d\Omega\}_{\text{av}}, \qquad (28)$$

where $q^{(\text{in})}_{(\text{upper})}$ and $q^{(\text{in})}_{(\text{lower})}$ are the total inelastic collision rates for the upper and lower level, respectively, v is the electron velocity, $f(\Omega)$ is the elastic scattering amplitude, and averge is taken over the electron velocity distribution. For the lines of the Lyman series the contribution to the width from the scattering on the lower level can be neglected and the FWHM is then simply equal to the sum of all (elastic and inelastic) collision rates for the scattering on the upper level. In our procedure, collision cross sections and rates were calculated in a distorted-wave approximation described in Ref. 5. The hypernetted-chain calculations for these plasma conditions indicate that the mutual interaction between the bound and the free electron is not affected by screening. We have used therefore the full Coulomb interaction of the two electrons in the evaluation of collision cross sections. The cross sections for the 2p-2s transition exhibit resonances in the low-energy region (Fig. 9) caused by

Table VI

Ratio A/A_c of transition probability coefficients

for hydrogen-like argon.

Pure argon plasma, T = 1000 eV.

Transition	$N_e = 5 \times 10^{24}$ cm^{-3}	$N_e = 2 \times 10^{25}$ cm^{-3}
2p-1s	0.994	0.969
3p-1s	0.835	
3p-2s	0.995	
3s-2p	1.140	
3d-2p	0.936	

the enhancement of the low partial waves. A similar behavior has been found previously[5] for hydrogenic neon and argon at different plasma conditions. The resonance appears to be caused by a temporary trapping of the colliding electron in a quasi-bound orbit just above the ionization limit.

Electron collision rates contributing to the perturbation of the 2p level are summarized in Table VII together with the FWHM of the Lyman α lines. It is to be noted that the 2p-2s collision rate represents a dominant contribution to the sum of inelastic collision rates and that its magnitude is due mainly to the small difference of the two levels as apparent from the $I_{n\ell}$ values in Table IV. Thus correct differences of energy levels are essential for the calculation of line widths. As mentioned before, energy differences derived from the values $I_{n\ell}$ in Table IV may not be directly observable and therefore suitable for the calculation of inelastic collision cross sections. A complete theory should include several other effects and also a time-dependent character of all processes involved in the emission of radiation. Therefore the derived value of the Lyman α width should be regarded only as an approximation.

The frequency of electron collisions with the H-like argon is at least two orders of magnitude larger than the spontaneous transition probability for the Lyman α line ($A = 6.5 \times 10^{13}$ sec^{-1}). Our assumption, which is implicit to the present treatment of hydrogen-like ions, that the distribution of free electrons will adjust to the various atomic orbitals $n\ell$, is therefore a reasonabale first approximation.

The frequency of plasma fluctuations is expected to be approximately equal to the plasma frequency, which, in our case, is equal to 2×10^{16} and 4×10^{16} sec^{-1}, respectively. Since the average lifetime due to collisions of the low excited state is of the same order of magnitude as the individual plasma fluctuations, the use of a time-averaged potential and a time-independent electron wave functions is not rigorously correct. For the time being it is an implicit assumption in our formalism that remains to be confirmed.

To conclude, there are a number of issues not directly addressed here but have bearing on the problem. It has been our intent to describe the effects of the plasma environment on the so-called isolated atom eigenfunctions and eigenvalues. In a steady-state situation we have

Table VII

Electron collision rates (sec^{-1}) for scattering on the

2p level of a hydrogen-like argon. Pure argon plasma, T = 1000 eV.

Inelastic collisions	$N_e = 5 \times 10^{24}$ cm^{-3}	$N_e = 2 \times 10^{25}$ cm^{-3}
2p-1s	2.39×10^{13}	9.26×10^{13}
2p-2s	2.58×10^{15}	1.78×10^{16}
2p-3s	2.84×10^{13}	
2p-3p	3.25×10^{24}	
2p-3d	5.35×10^{14}	
All inelastic collisions	3.49×10^{15}	1.79×10^{16}
All elastic collisions	1.95×10^{15}	8.69×10^{15}
Total collision rate	5.44×10^{15}	2.66×10^{16}
L_α collision width (FWHM)	22.5 eV	110.0 eV

accomplished this. A new basis set has been derived from which a number of atomic parameters can be obtained. In addition, through the proper choice of a time-development operator it should be possible to describe the time evolution of these parameters as well as calculate some of the more relevant physical observables, such as line shifts. The evaluation of these quantities is presently under investigation and will be reported on later. However, this should in no way detract from what has been accomplished here. In fact, for a variety of cases and conditions it may very well be that 2nd order terms calculated in our new basis set are negligible.

Acknowledgment

We would like to acknowledge helpful discussions with Forrest Rogers as well as stimulating discussion with Dr. Jinx Cooper. This work was supported by the Office of Naval Research.

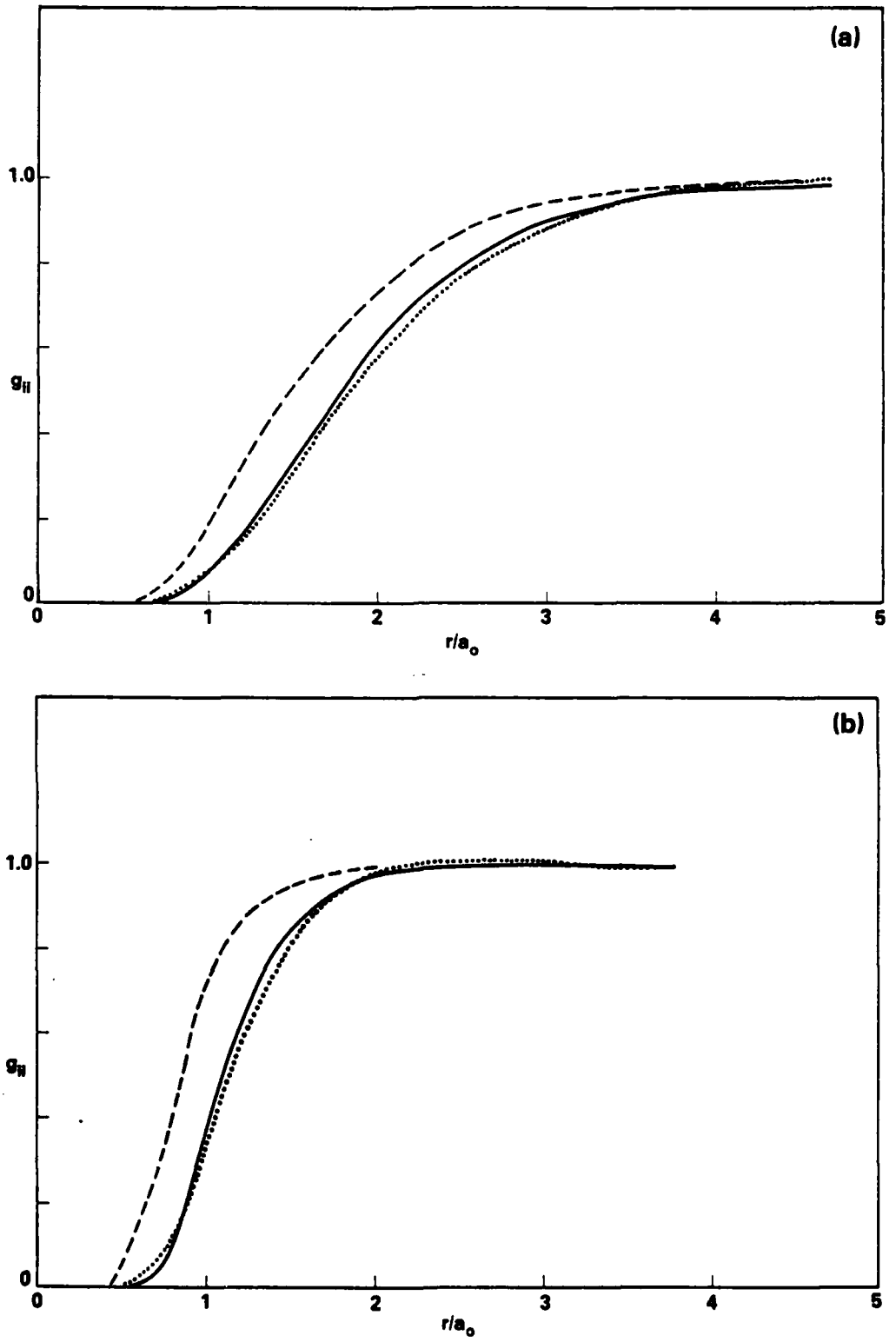

Fig. 1. Ion-ion radial distribution functions for (a) $\Gamma = 2.2$ and (b) $\Gamma = 4.9$ in HNC (dots), DFM (solid line), and DH (dashed line) approximations. The distance r is in units of the Bohr radius, a_o.

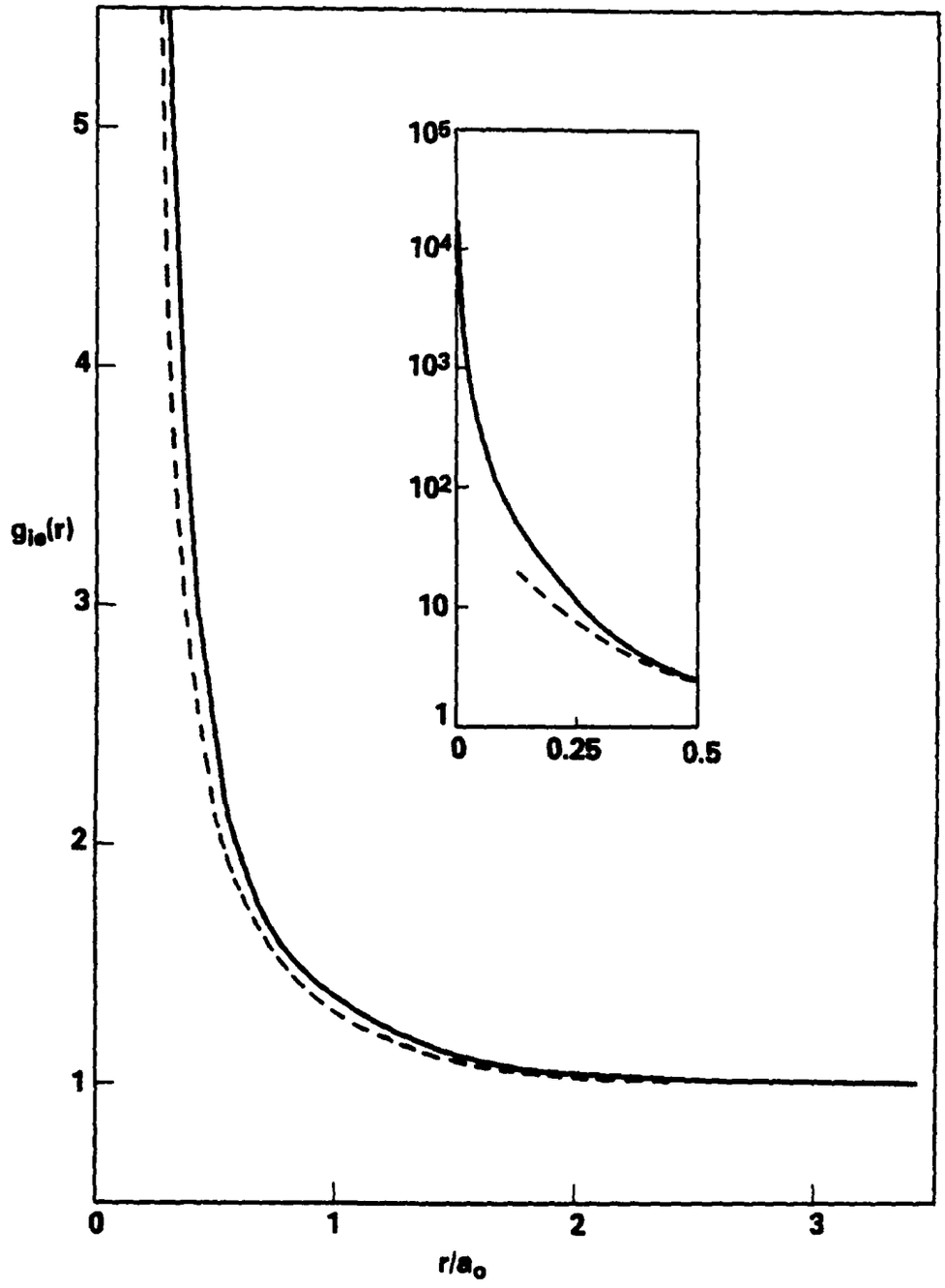

Fig. 2. Electron distribution around an ion for $\Gamma = 2.2$. Solid line is the DF model; dashed is the HNC approximation. The smallest radius used in the Fourier transform within the HNC scheme was $r/a_o = 0.125$.

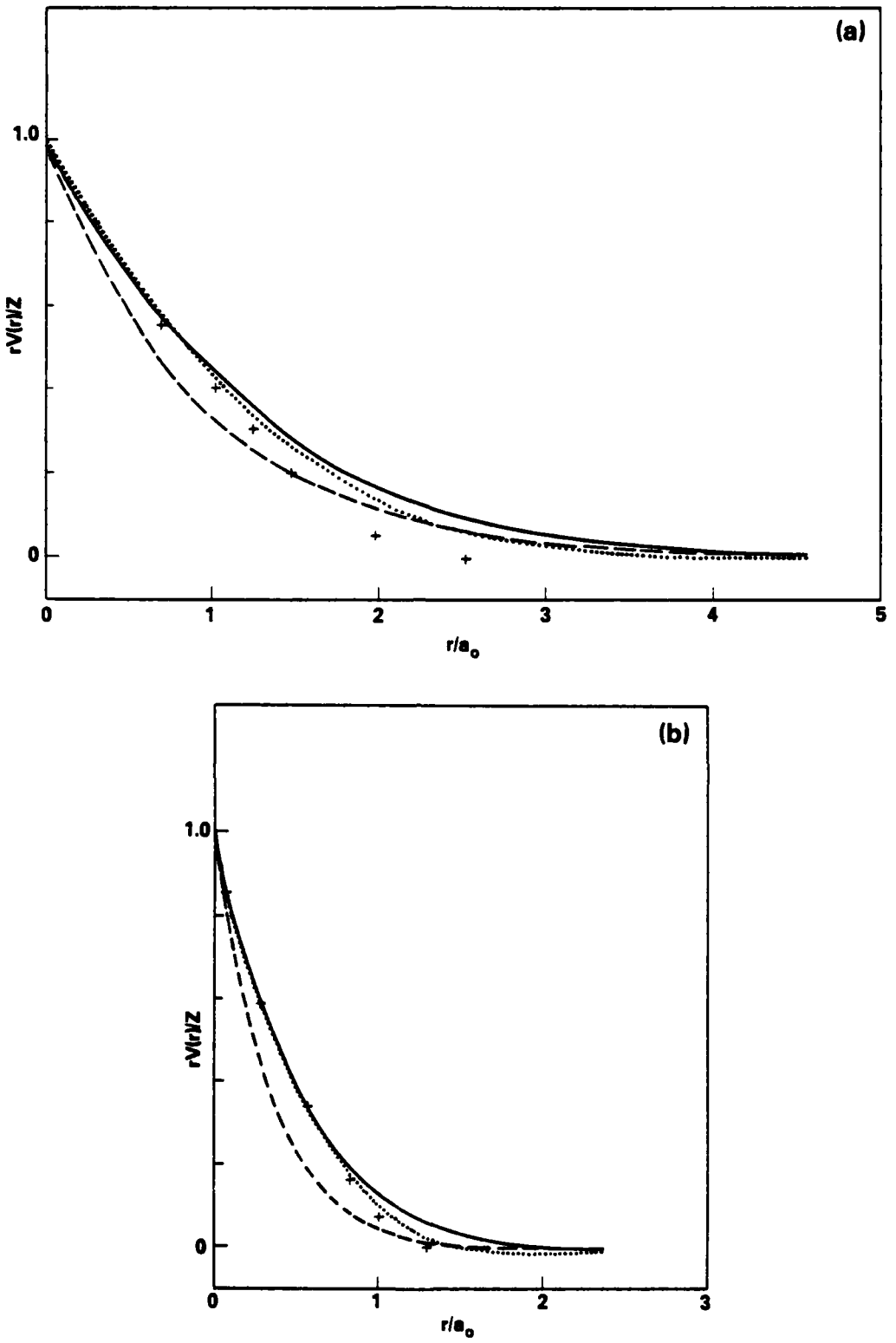

Fig. 3. Effective electron-ion potentials resulting from the DF model (solid), HNC/Poisson model (dots), ion-sphere model (crosses), and DH theory (dashes) for (a) $\Gamma = 2.2$ and (b) $\Gamma = 4.9$.

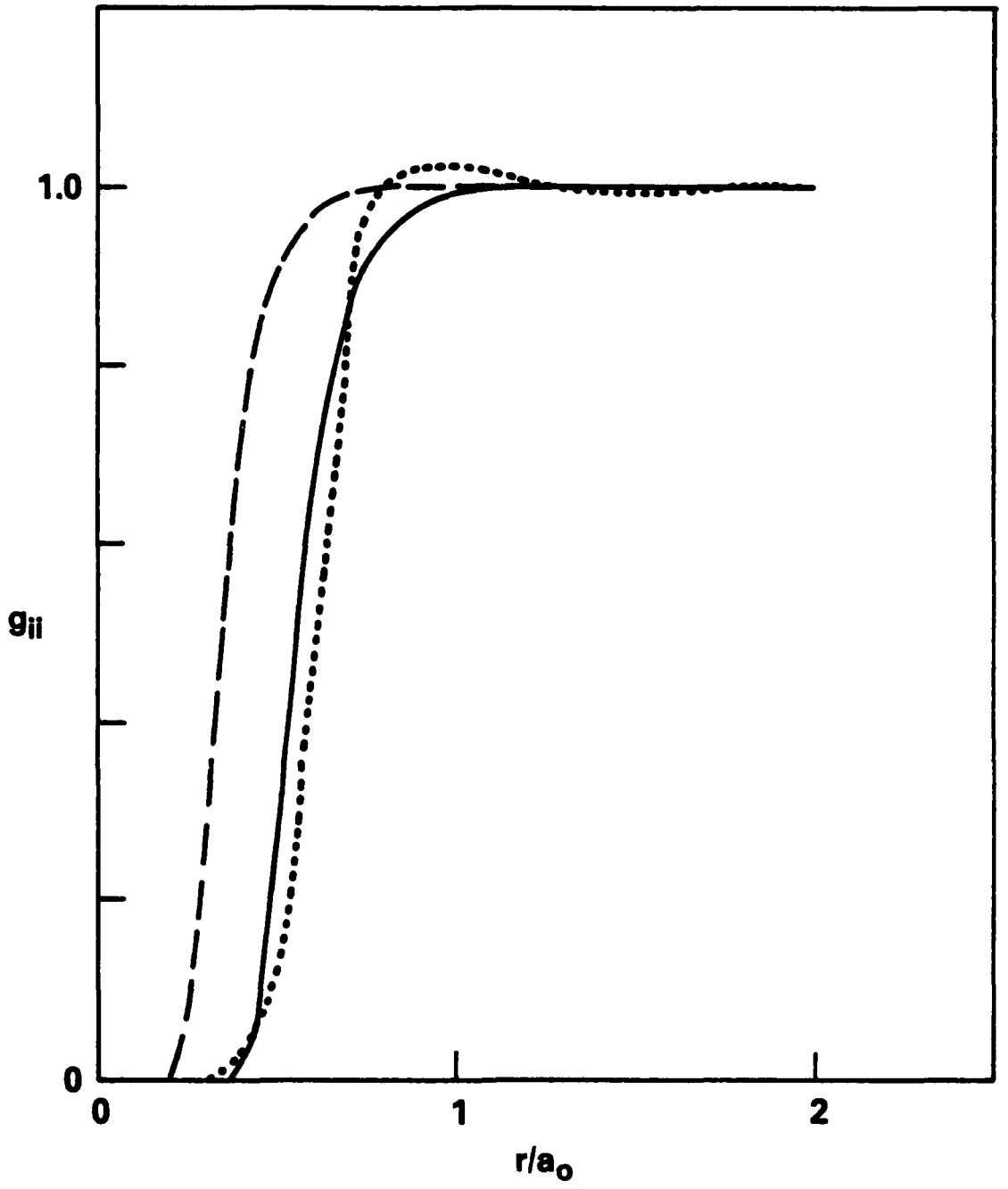

Fig. 4. Ion density distribution function for the $\Gamma = 13.1$ case in three approximations. The legend is the same as Fig. 1.

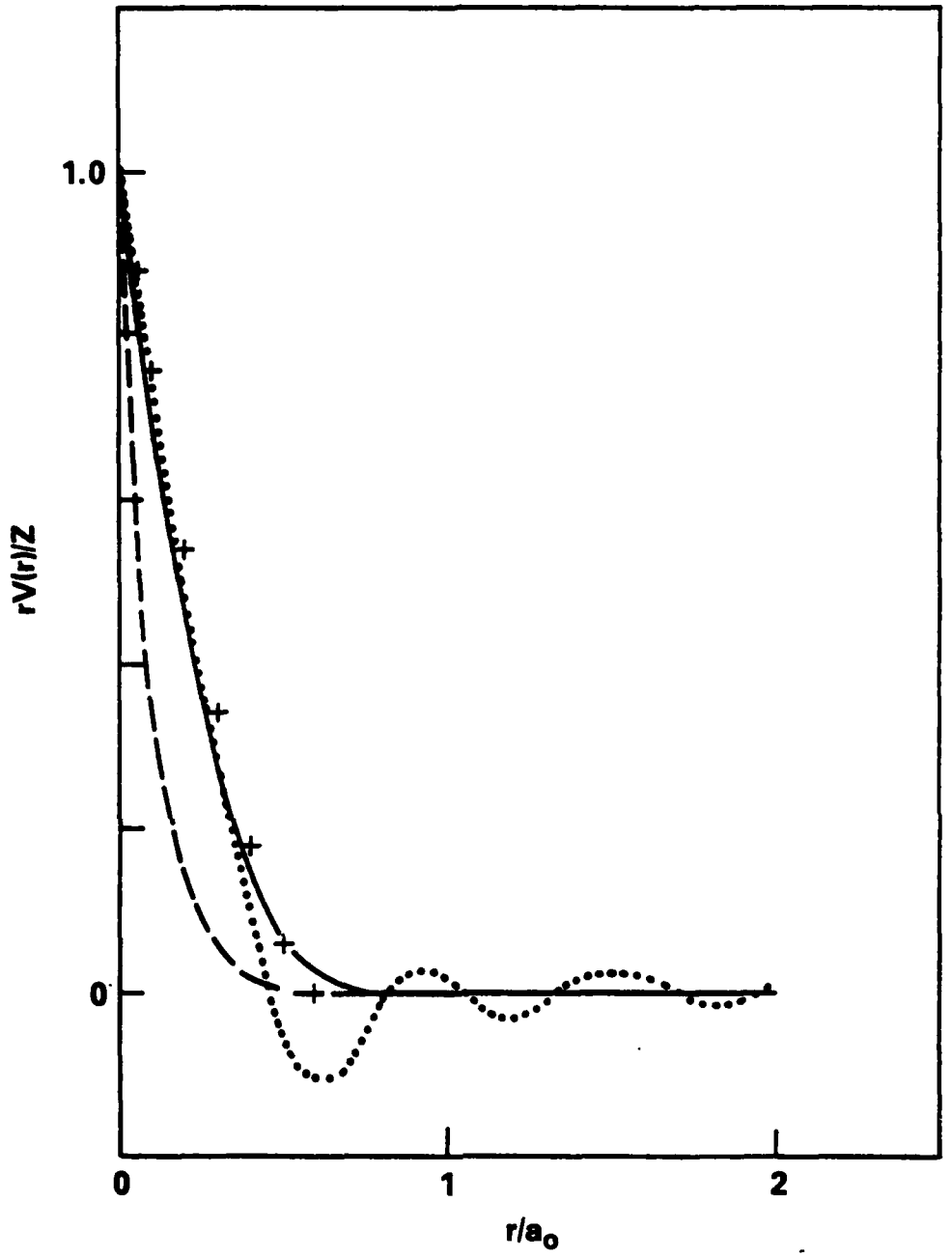

Fig. 5. Effective electron-ion potential for Γ = 13.1 neon. The legend is identical to Fig. 3.

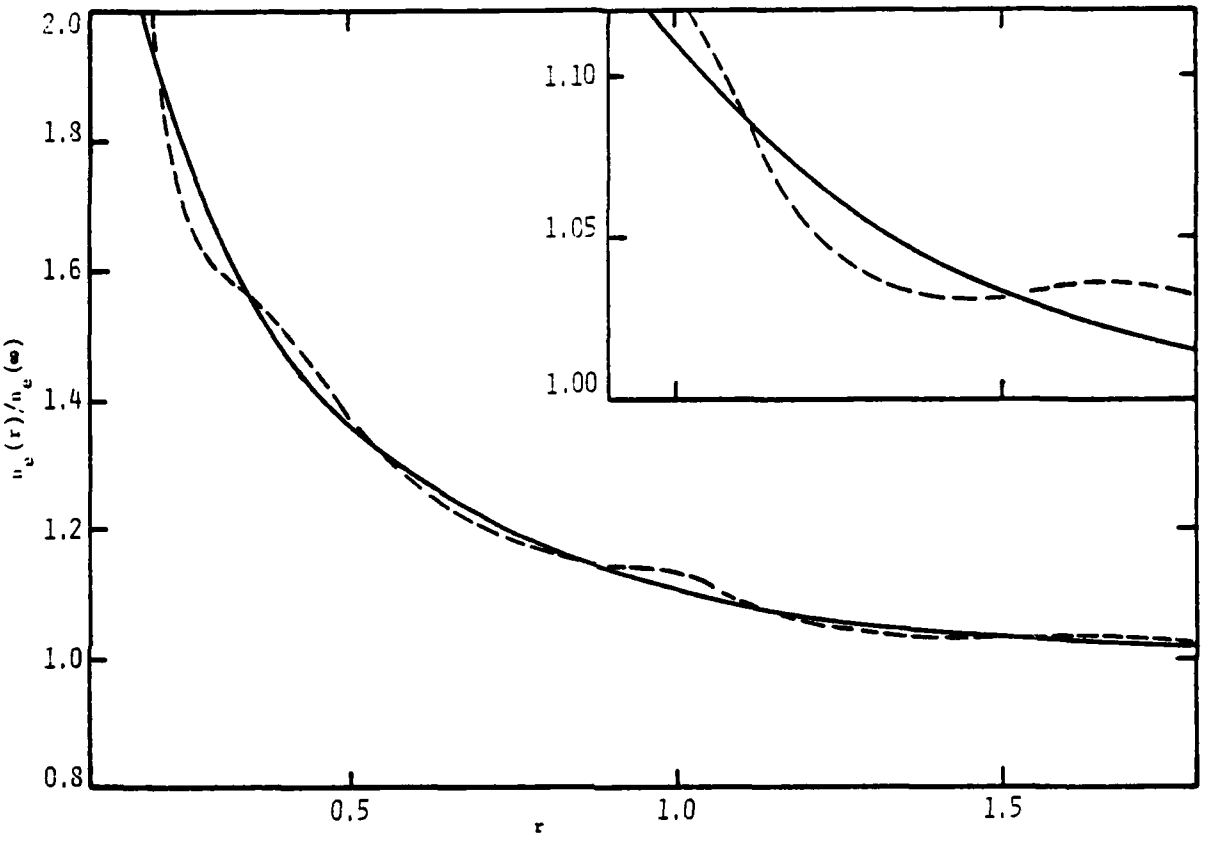

Fig. 6. Electron density distribution around a fully stripped argon ion in a pure argon plasma, T = 1000 eV, $N_e = 5 \times 10^{24}$ cm^{-3}. Solid curve - n_e from eq. (22); dashed curve - n_e from (15) and (17).

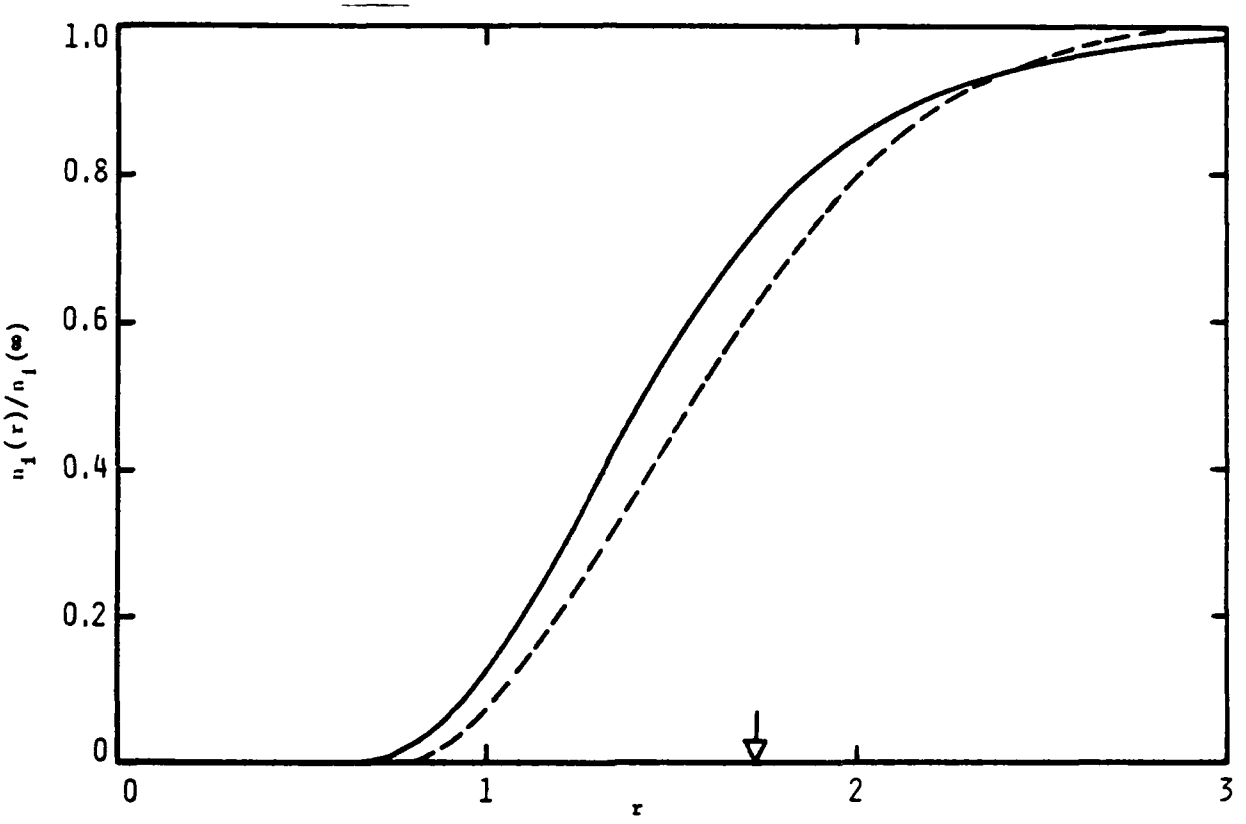

Fig. 7. The distribution of ions about a given ion according to eq.(19) for pure argon plasma, T = 1000 eV, N_e = 5 x 10^{24} cm^{-3}. Solid curve - average atom model; dashed curve - hypernetted chain approximation with $\overline{Z}$ = 16.08. Arrow indicates the ion sphere radius.

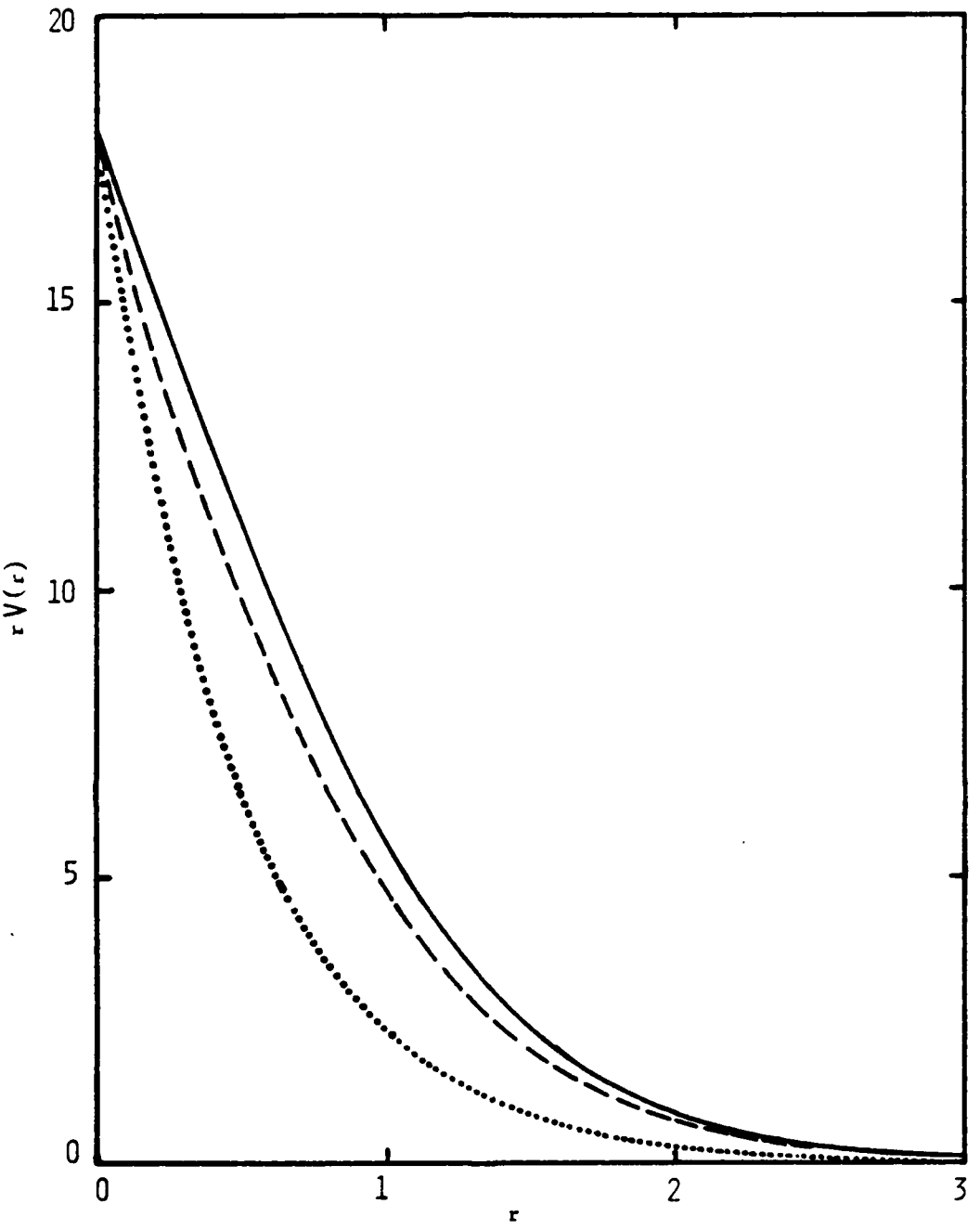

Fig. 8. Comparison of potentials V(r) defined by (20) for pure argon plasma, T = 1000 eV, $N_e = 5 \times 10^{24}$ cm^{-3}. Solid curve - fully stripped argon; dashed curve - average atom model; dotted curve - linearized Debye-Hückel potential with Z = 18, $\bar{Z} = 16.08$. Potential curves for hydrogen-like argon lie between the solid and dashed curves.

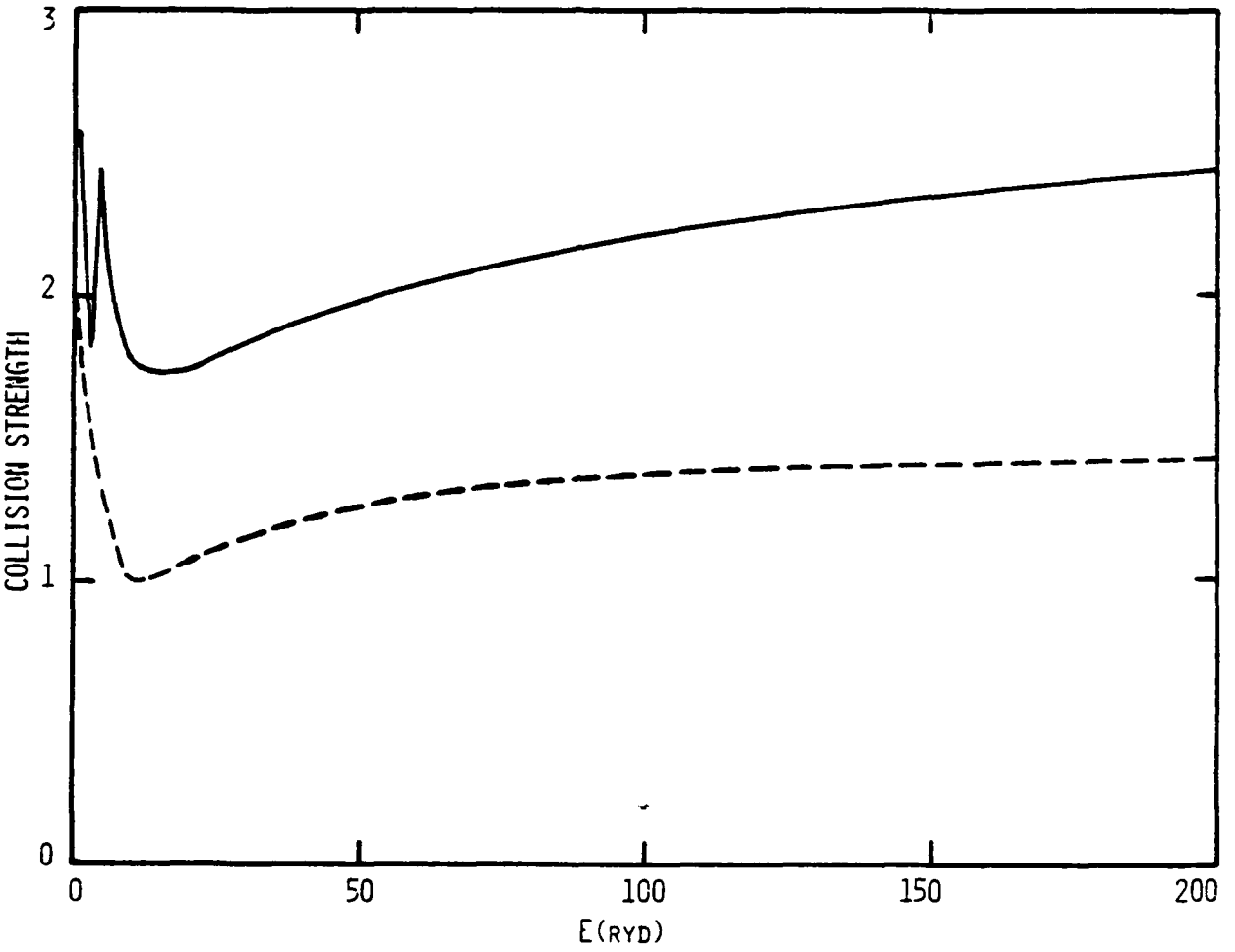

Fig. 9. Electron collision strengths for the 2p-1s transition in hydrogen-like argon. Pure argon plasma, T = 1000 eV. Solid curve - $N_e = 2 \times 10^{25}$ cm^{-3}; dashed curve - $N_e = 5 \times 10^{24}$ cm^{-3}. E = energy of incident electrons.

References

1. R.D. Cowan and J. Ashkin, Phys. Rev. 105, 144 (1957).
2. Balazs R. Rozsnyai, Phys. Rev. A5, 1137 (1972).
3. J.C. Weisheit, PPPL-1765 (1981), to appear in Applied Atomic Collision Physics, Vol. II, Ed. H. S. Massey.
4. S. Skupsky, Phys. Rev. A21, 1316 (1980).
5. J. Davis and M. Blaha, Physics of Electronic and Atomic Collisions, Ed. S. Datz (North-Holland, New York, 1982).
6. U. Gupta and A.K. Rajagopal, Phys. Rep. 87, No. 6 p. 259 (1982).
7. U. Gupta, M. Blaha, and J. Davis (to be published in J. Phys. B.).
8. J.P. Hansen, Phys. Rev. A8, 3096 (1973).
9. M. Baus and J-P. Hansen, Phys. Rep. 59, 1 (1980); S. Ichimaru, Rev. Mod. Phys. 54, 1017 (1982).
10. C. Deutsch, Phys. Lett. 60A, 317 (1977).
11. J.P. Hansen and I.R. McDonald, Phys. Rev. A 23, 2041 (1981).
12. J.F. Springer, M.A. Pokrant, and F.A. Stevens, Jr., J. Chem. Phys. 58, 4863 (1973).
13. F. Rogers, UCRL-89123 (1983), to appear in Phys. Rev. A.
14. R. Kubo, J. Phys. Soc. Jap. 12, 570 (1957).
15. R. M. More, UCRL-88511 (1982), to appear in Atomic and Molecular Proceses in Controlled Fusion, proceedings.
16. S.G. Brush, H.L. Sahlin, and E. Teller, Phys. Rev. 45, 2102 (1966).
17. M.W.C. Dharma-wardana, J. Quant. Spect. Rad. Transf. 27, 315 (1982).
18. See, e.g., Fig. 1 of Ref. 5 for comparison.
19. M. W. C. Dharma-wardana and R. Taylor, J. Phys. C.: Solid St. Phys. 14, 629 (1981).
20. R. D. Cowan, The Theory of Atomic Structure and Spectra, Univ. of California Press, 1981.
21. J. Stewart and K. Pyatt, Jr., Astrophys. J. 144, 1203 (1966).

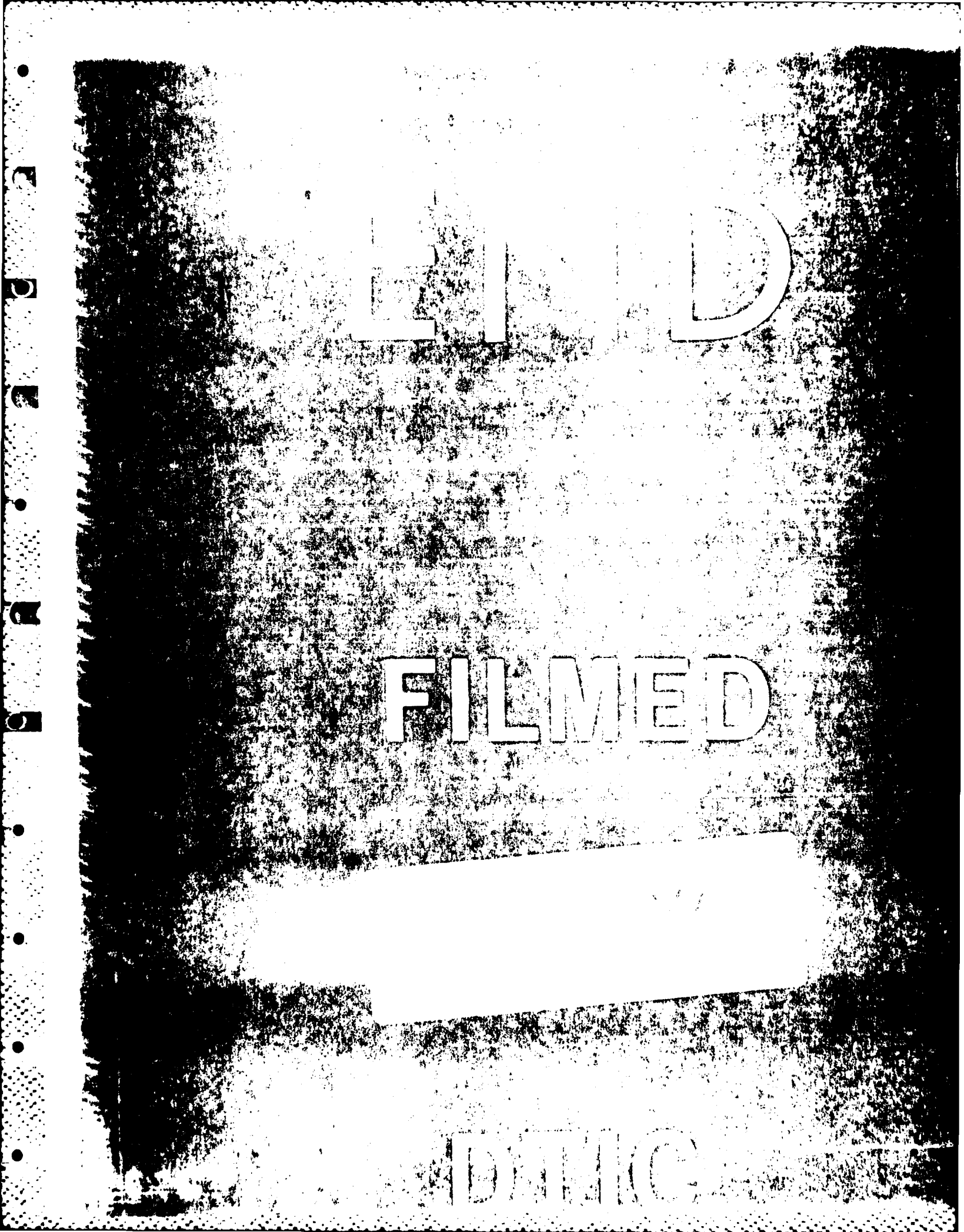
FILMED